Geophysical Journal International

Geophys. J. Int. (2020) **220,** 190–200
Advance Access publication 2019 September 30
GJI Geomagnetism, rock magnetism and palaeomagnetism

doi: 10.1093/gji/ggz432

Deformation of rhyolite lava crust associated with intermittent inner flow of lava: palaeomagnetic evidence

Koji Uno,[1] Kuniyuki Furukawa,[2] Kotaro Nakai,[1] Takuma Kamio[1] and Tatsuo Kanamaru[3]

[1]*Department of Earth Sciences, Okayama University,* 3-1-1 *Tsushimanaka, Kita-ku, Okayama* 700-8530*, Japan. E-mail: unokoji@okayama-u.ac.jp*
[2]*Faculty of Business Administration, Aichi University,* 4-60-6 *Hiraike-cho, Nakamura-ku, Nagoya* 453-8777*, Japan*
[3]*Department of Earth and Environmental Sciences, Nihon University,* 3-25-40 *Sakurajosui, Setagaya-ku, Tokyo* 156-8550*, Japan*

Accepted 2019 September 26. Received 2019 September 17; in original form 2019 April 10

SUMMARY

A palaeomagnetic study has been conducted to examine the deformation of thick crusts of rhyolite lava while its inner portions continue to flow. The Sanukayama rhyolite lava, which erupted in the Pleistocene in Kozushima Island, Japan, was chosen as the investigation site because of its well-exposed vertical lithofacies variations classified into three distinct zones (pumiceous, obsidian and crystalline). The targets of this study are the pumiceous and obsidian zones, which constitute the crust of the lava. Thermal demagnetization reveals three remanent magnetization components from the pumiceous and obsidian samples but only a single magnetization component from the inner crystalline rhyolite samples. Alternating field demagnetization is ineffective in isolating the magnetization components in the pumiceous and obsidian samples. The multiple components of remanent magnetization of the crust are interpreted to have been acquired during cooling as thermoremanent magnetizations. We suspect intermittent lava transport of the inner portions, the primary mode of rhyolite lava advancement, to be responsible for the presence of multiple components in pumice and obsidian of the lava crust. When the inner portions of the lava retain mobility to flow out of the crust, the solidified crust of the lava surface below the magnetite Curie temperature remains susceptible to deformation. Analysis of palaeomagnetic directions from the crust allows the deformation of the crust to be described in terms of rotation. Although the mode of rhyolite lava advancement is not well understood, because of its infrequent occurrence, our observations offer an important insight on how the mobile part of the lava is associated with the deformation of the crust during continued lava advance.

Key words: Asia; Palaeomagnetism; Rock and mineral magnetism; Volcanic hazards and risks.

1 INTRODUCTION

Low-viscosity lava flows, such as basaltic lava, form a solidified crust due to the cooling of the lava surface while lava underneath continues to flow. The solidified crust insulates the lava and prevents its inner temperature from rapidly decreasing, enabling the inner flow to continue for longer periods (e.g. Calvari & Pinkerton 1998). For andesitic and dacitic lava, this type of flow is uncommon. Crystal-poor rhyolitic lava may become significantly less viscous than crystal-rich andesitic or dacite lava (Magnall *et al*. 2017), leading to such crustal control to be observed. The 2011–2012 Cordón Caulle eruption in Chile was a recent eruption event in which the process of rhyolitic lava emplacement was observed in detail for the first time. Observations confirmed that the lava continued to spread extensively for more than 6 months after the supply of lava from the vent ceased. The lava spread more widely as more mobile lava beneath the crust, intermittently flowing out (breakout) at the distal ends in several locations (Tuffen *et al*. 2013; Farquharson *et al*. 2015; Magnall *et al*. 2018). This observation suggests that the solidified crust of the lava surface remains susceptible to deformation for a long time, as it is affected by the long-term inner flow of lava that is inferred from several months to years (Anderson & Fink 1990; Griffiths 2000). Crustal deformation can create pathways for hazardous lava breakouts; therefore, it is imperative to understand this type of crustal deformation behaviour to evaluate the potential risks related to volcanic hazards associated with silicic eruptions.

We conducted a palaeomagnetic study on a thick rhyolite formation to examine the deformation behaviour of thick crusts (the upper glassy part of the lava) that may occur in response to lava transport of the inner portions (microcrystalline material with commonly observed spherulites). In the case of the most recent

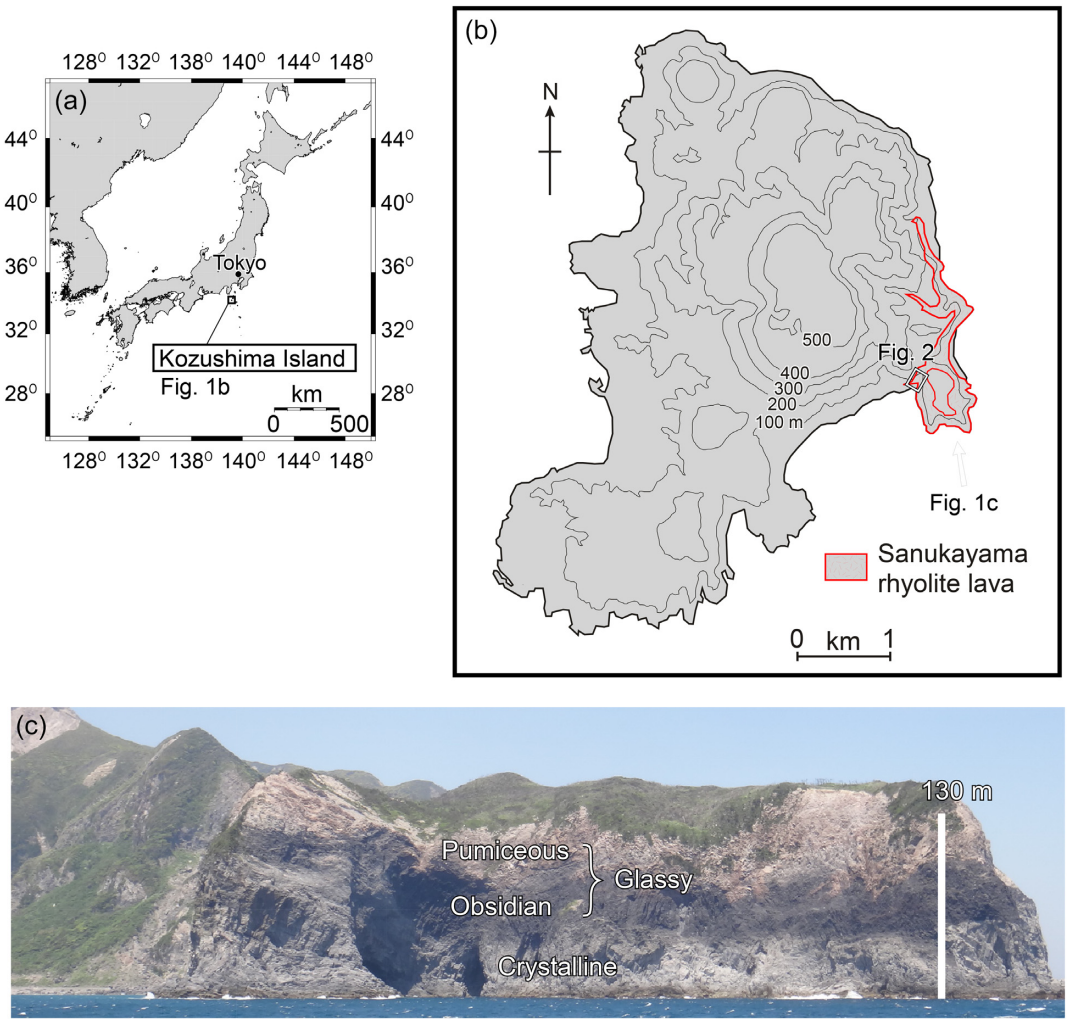

Figure 1. (a) Outline map of the Japanese Islands showing the location of Kozushima Island. (b) Topographic map of Kozushima Island showing the distribution of the Sanukayama rhyolite lava. The rest of the island consists of lava and pyroclastic flow deposits of various ages. (c) Photograph of the Sanukayama lava section exposed in the sea cliff.

Cordón Caulle eruption, such investigation cannot be conducted on the Cordón Caulle 2011–2012 lava because the lava has not eroded enough for the internal texture to be studied. The Sanukayama rhyolite lava, which erupted in the Pleistocene in Kozushima Island, Japan (Fig. 1a), was chosen as the site of our investigation. The Sanukayama lava is well eroded and the internal texture extremely well exposed, enabling us to illustrate deformation features in the vertical perspective. A thick crust of about 80–100 m of the rhyolite lava would provide long-term insulation of the inner portions and provides an opportunity to observe the crustal deformation history. A glass transition temperature of the Sanukayama lava based on the composition (about 76 wt per cent SiO_2) and H_2O content (1 per cent) is estimated to be 860 °C, according to Giordano *et al.* (2008). Because this value is higher than the Curie temperature of magnetite (580 °C), the deformation history after the crust has cooled below this temperature is assumed to be recorded. Here, we observed that the rhyolitic crust suffered at least two phases of deformation, through the thickness of ∼80 m, during cooling, most likely in association with intermittent internal lava transport.

2 SANUKAYAMA RHYOLITE LAVA

The Sanukayama rhyolite lava is exposed on the eastern edge of Kozushima Island, Japan (Fig. 1b). The distribution of the lava measures 2 km in length (north–south) and 0.6 km in width (east–west) (Isshiki 1982). This lava is estimated to have moved southward, based on a palaeoslope analysis (Furukawa *et al.* 2019). Kaneoka & Suzuki (1970), Fukuoka & Iso (1980) and Sugihara & Danhara (2008) dated the lava at 70 ± 5, 51 ± 4 and 110 ± 30 ka, respectively, using fission track dating. Taniguchi (1980) reported an age of 60–79 ka based on hydration layer glass dating. Yokoyama *et al.* (2004) used electron spin resonance (ESR) dating to determine ages of 46 ± 3 and 68 ± 5 ka based on Al and Ti–Li centre signal, respectively. Bulk chemical composition of the lava was analysed to be 76.5 wt per cent SiO_2 (Furukawa *et al.* 2019). The vertical section of the Sanukayama lava, maximum thickness of about 130 m, is very well exposed along a sea cliff (Figs 1b and c). The lithofacies of this section are classified into crystalline, obsidian, and pumiceous zones from the bottom to the top (Fig. 1c). The latter two correspond to the upper glassy part reported in various regions of rhyolite lava flow (Fink & Manley 1987; Manley & Fink 1987;

Furukawa & Kamata 2005). No clinker layer is observed in the lava, suggesting that the lava was formed in one event. In the obsidian zone, there is a well-developed, nearly horizontal, clastic layer with a sintered matrix <80 cm wide and >20 m long (Furukawa *et al*. 2019). The layer margin tapers down to a termination point and the layer slightly undulates, indicating post-formation ductile deformation. Isshiki (1982) inferred from the lithofacies that the upper half of the entire lithofacies in the Sanukayama section is estimated to be above the present ground level, and that the actual lava thickness may reach 300 m; however, the lava below sea level may be thinner as crystallization has been suppressed within the inner part of the crust. The lava, at least the exposed part, is inferred to be formed under a subaerial environment because there is no evidence of interactions with water such as marginal hyaloclastites, branched lava lobes, polyhedral fragments, or peperites (Furukawa *et al*. 2019). Furthermore, in the exposed part, we infer no significant increase in cooling rate as a result of external water ingress, as there is no closely spaced or columnar jointing in the dense obsidian. The surface morphology of the lava is obscured by the deposition of the Chichibuyama pyroclastic rocks emplaced at about 20 ka (Suga *et al*. 1992), and the contact between the pumiceous lava section and the overlying rocks has undergone little erosion.

Palaeomagnetic sampling was conducted at an exposure of the cliff that had been scraped off to form a valley, which enabled us to access the interior portion; the locality east of the valley is referred to as the east wall, and the locality to the west as the west wall (Fig. 2a). Palaeomagnetic sampling sites are distributed among the pumiceous and obsidian zones, and also distributed in both walls. Samples from the pumiceous zone were collected at seven sites (Fig. 2b). Samples from the obsidian zone were collected at four sites (Fig. 2b), including one clastic layer site from which palaeomagnetic data were previously obtained by Furukawa *et al*. (2019). These sampling sites were distributed over a thickness of about 80 m. In addition, samples of the crystalline zone were collected for comparison from two sites. All samples were obtained as hand samples and were oriented in the field using a tripod-mounted magnetic compass to maintain a distance from the rock surface. Based on the condition of outcrops, 4, 5, 7, 8, 9 and 10 hand samples were collected at sites 2, 1, 3, 4, 1 and 2, respectively. The present-day geomagnetic field declination at the sampling sites was determined using the International Geomagnetic Reference Field model (Finlay *et al*. 2010).

3 METHODS

In the laboratory, each oriented hand sample was cored and cut into cylindrical specimens with diameters of 25 mm and lengths of 22 mm. Natural remanent magnetizations (NRMs) were measured with a Natsuhara SMM-85 spinner magnetometer at Okayama University. All samples were subjected to progressive thermal demagnetization treatment using a Natsuhara TDS-1 thermal demagnetizer. Progressive demagnetization is characterized by progressively heating specimens from ambient temperature to the Curie temperature of magnetic minerals, such as magnetite, to emulate the natural cooling process of hot lava, in the laboratory, but in a reverse way (Uehara *et al*. 2015). At each demagnetization step, the intensity and direction of remanent magnetization are measured. Thermal demagnetization is performed until the magnetization is eliminated. The magnetic vector information is useful to verify whether the trajectory of the magnetization vector for a sample is linear throughout demagnetization, which would indicate no deformation (tilting or rotation) for the sample below the Curie temperature. The trajectory of the vector shows multiple linear segments demarcated with angles, which indicate deformation during cooling at separation temperatures between the two successive vectors. When three linear segments are observed during thermal demagnetization from room temperature, they are generally termed as low-, medium-, and high-temperature components according to the order of appearance. Progressive thermal demagnetization in this study is performed in a series of 50 °C steps between 100 and 300 °C, 40 °C steps between 300 and 500 °C and 10–20 °C steps above 500 °C.

Selected samples were subjected to progressive alternating field (AF) demagnetization treatment using a Natsuhara DEM-95 AF demagnetizer in a series of 2.5 mT steps between 2.5 and 10 mT, 5 mT steps between 10 and 40 mT, and 10 mT steps between 40 and 60 mT, to compare the demagnetization behaviour between the two methods.

Results for each sample were plotted on orthogonal vector diagrams (Zijderveld 1967) to evaluate demagnetization behaviour (Fig. 3). Principal component analysis (Kirschvink 1980) was used to estimate directions of the observed magnetic components. Palaeomagnetic data were analysed using the software applications developed by Hatakeyama (2018).

Progressive thermal demagnetization of a three-component isothermal remanent magnetization (IRM) (Lowrie 1990)—in fields of 2.5 T (high-coercivity component), 0.4 T (medium-coercivity component), and 0.12 T (low-coercivity component)—was performed using a Magnetic Measurements MMPM10 pulse magnetizer at Okayama University. The modified Lowrie–Fuller test (Johnson *et al*. 1975)—anhysteretic remanent magnetization (ARM) in 0.1 mT steady field and 0.1 T alternating field, and saturation IRM in the 0.2 T field—was also performed using a Natsuhara ARM coil attached to the AF demagnetizer at Okayama University. A JEOL JXA8800 electron probe microanalyser at Nihon University was used to identify the chemical compositions of iron oxides. Operating conditions were a 12 nA beam current, 15 kV accelerating voltage, and a beam diameter of 5 μm.

4 RESULTS

Initial NRM intensities range between 1.6×10^{-2} and 72 A m^{-1}, with the majority at the order of 1 A m^{-1}. Samples of crystalline parts have higher intensities (mean of 3.7 A m^{-1}), while those of pumiceous parts have lower intensities (mean of 2.3×10^{-1} A m^{-1}). The number of remanent magnetization components observed during thermal demagnetization essentially depends on stratigraphic position: glassy (obsidian and pumiceous) or crystalline (Table 1). Following unblocking of unstable magnetization in the first several steps of thermal demagnetization, a single remanent magnetization component was observed at sites in the crystalline zone (KZ1 and KZ19; Fig. 3a). On the contrary, three components of remanent magnetization were recognized at sites in the obsidian (KZ2 and KZ20) and pumiceous zones (KZ8, KZ9, KZ10, KZ15, KZ17 and KZ21; Figs 3c–e). A site in the clastic layer in the obsidian zone (KZ11) yields a single remanent magnetization component (Fig. 3g), and also, another site in the obsidian zone that is in contact with the upper boundary of the clastic layer (KZ16) shows only a single remanent magnetization component (Fig. 3h). The remaining pumiceous site (KZ18) displays erratic directional behaviour with no stable endpoints during thermal demagnetization. The samples from this site are fractured, likely resulting from their proximity to a tectonic fault (Taniguchi 1977).

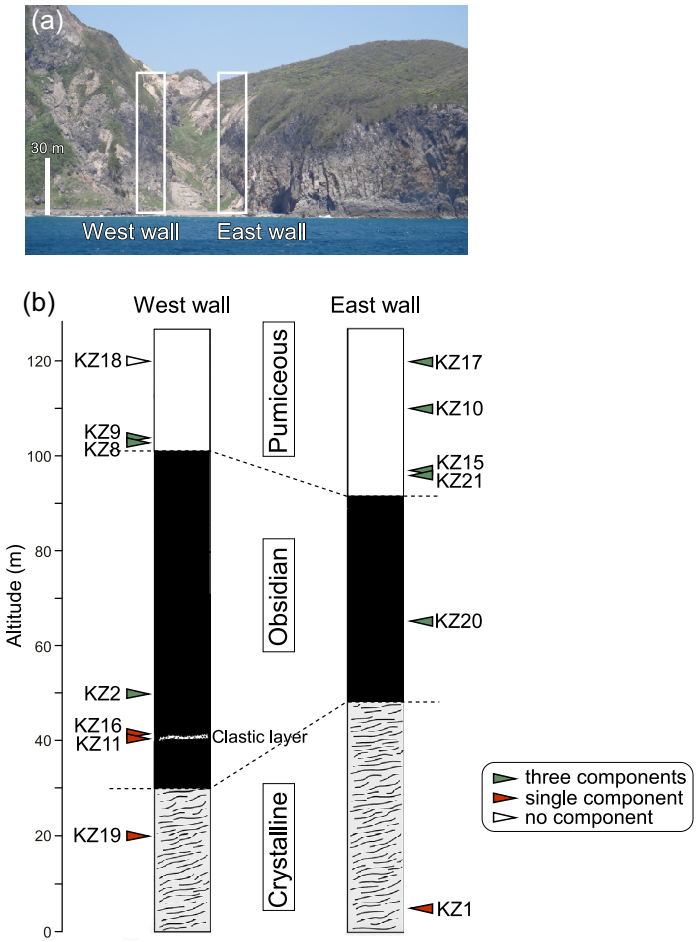

Figure 2. (a) Photograph of the palaeomagnetic sampling area that is scraped off to form a valley. (b) Schematic columns of the west and east walls showing stratigraphic horizons of palaeomagnetic sampling sites.

4.1 Crystalline zone

Crystalline samples with a single component of remanent magnetization show linear decay in the orthogonal vector diagrams above about 250 °C. The large decay in intensity is observed around 500 °C. The most commonly observed laboratory unblocking temperature range for this component is between 560 and 580 °C (Fig. 3a). The unblocking temperature is the temperature at which the remanent magnetization for a sample is completely removed by thermal demagnetization. Magnetite is expected to have a maximum unblocking temperature of about 580 °C, and the addition of titanium (i.e. titanomagnetite) will reduce the unblocking temperature of a sample (e.g. Lowrie 1990). Magnetization with unblocking temperatures above 560°C is generally regarded as being carried by Ti-poor titanomagnetite. The observed remanent magnetization is therefore carried by Ti-poor titanomagnetite, confirmed by chemical composition analysis (Table 2). Progressive AF demagnetization up to 60 mT also allows identification of a single magnetization component (Fig. 3b). Thermal demagnetization of the three-component IRM shows that the low-coercivity (0.12 T) magnetization is dominant and is completely unblocked by 580 °C (Fig. 4a), suggesting that remanent magnetization predominantly resides in titanomagnetite.

The mean direction is well defined for crystalline sites. The precision parameters (k value) of the mean directions are 64.0 (KZ1) and 347.5 (KZ19). The directions are of north declination with intermediate positive inclination and are close to each other (Fig. 5a, Table 1).

4.2 Obsidian and pumiceous zones

Obsidian and pumiceous samples with multiple components of remanent magnetization show three linear segments demarcated at a certain angle in the orthogonal vector diagrams (e.g. Fig. 3c). The higher the altitudes of the sampling sites, the lower the temperatures at which the components are separated. For example, site KZ2 at 48 m altitude exhibits temperatures of separation of the magnetization components at 520 and 550 °C, while site KZ17 at 120 m altitude shows separation at 460 and 540 °C (Figs 2b, and 3d and e). The remanent magnetization is largely unblocked by about 580 °C. A small fraction of the magnetization remains unblocked above 580 °C and is demagnetized by 610 °C. The remanent magnetization largely resides in titanomagnetite, with small contributions from haematite and/or maghaemite (McIntosh 1991; de Boer *et al.* 2001). Progressive AF demagnetization is completely ineffective in isolating multiple components of the remanent magnetization (Fig. 2f). Thermal demagnetization of the three-component IRM shows that the low-coercivity magnetization is unblocked by 580 °C (Figs 4b and c), and a small fraction of high-coercivity (2.5 T) magnetization unblocked by 680 °C is also observed (Fig. 4c). Chemical composition analysis of iron oxide grains in an obsidian sample (KZ2–1) with a laboratory unblocking temperature of 560 °C shows

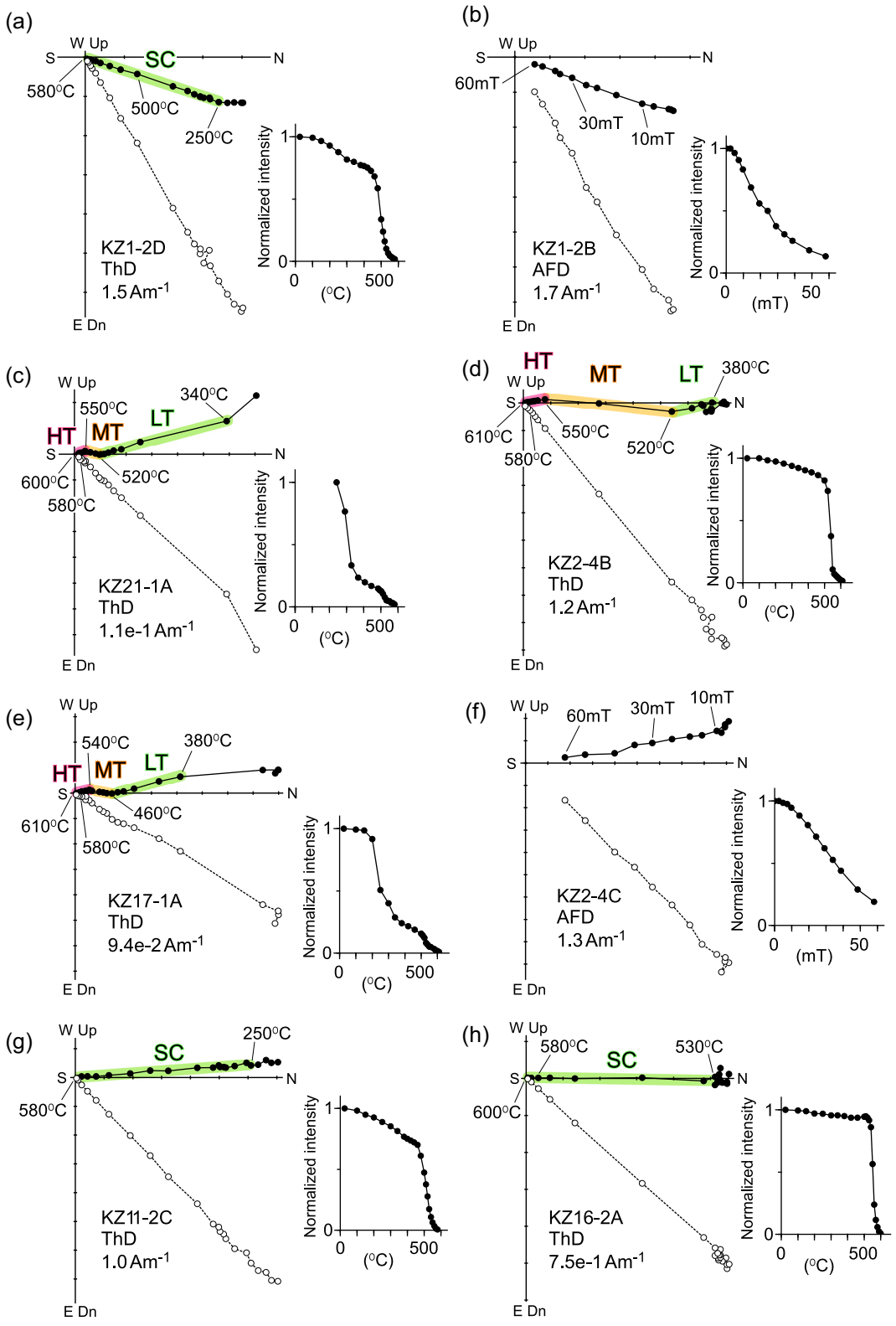

Figure 3. Representative orthogonal vector diagrams of thermal demagnetization and normalized remanence intensity curves. Solid and open symbols on orthogonal plots represent projections on the horizontal and vertical planes, respectively. SC: single magnetization component; LT: low-temperature component; MT: medium-temperature component; HT: high-temperature component. ThD: thermal demagnetization; AFD: alternating field demagnetization.

Table 1. Palaeomagnetic results of the Sanukayama rhyolite lava. *N*: the number of the samples in calculation for the means; *D* and *I*: declination and inclination, respectively; *k:* the precision parameter; α_{95}: radius of the cone of the 95 per cent confidence. Mean direction of the low-temperature component ($N = 8$) is calculated using directions from sites KZ2, 8, 9, 10, 15, 17, 20 and 21.

	Site	Single component					Low-temperature component					Medium-temperature component					High-temperature component				
		N	*D* (°)	*I* (°)	α_{95} (°)	*k*	*N*	*D* (°)	*I* (°)	α_{95} (°)	*k*	*N*	*D* (°)	*I* (°)	α_{95} (°)	*k*	*N*	*D* (°)	*I* (°)	α_{95} (°)	*k*
Crystalline																					
	KZ1	8	0.8	45.4	7.0	64.0															
	KZ19	7	355.4	46.8	3.2	347.5															
Glassy																					
Pumiceous zone	KZ8						8	350.0	51.3	6.5	74.6	8	0.3	48.5	6.0	84.9	8	348.5	51.0	6.1	82.8
	KZ9						5	337.2	48.0	7.9	94.8	5	11.4	47.2	10.2	57.2	4	351.3	46.7	9.3	98.6
	KZ10						7	331.4	60.0	10.4	35.0	7	345.6	62	8.2	54.6	4	302.2	54.1	10.1	83.8
	KZ15						7	9.8	34.4	4.8	156.2	7	26.2	42.5	8.2	55.2	7	9.3	36.4	4.8	158.5
	KZ17						4	353.0	36.8	17.8	27.5	4	10.7	52.2	13.7	45.8	4	347.7	37.0	17.2	29.5
	KZ18							—	—				—	—				—	—		
	KZ21						2	345.9	39.6			2	8.2	49.0			2	343.4	42.5		
Obsidian zone	KZ2						5	338.7	47.6	10.1	53.0	7	2.6	46.2	5.1	141.2	3	348.2	48.4	5.0	612.9
	KZ11	4	353.5	46.3	5.1	331.0															
	KZ16	4	347.1	41.5	12.0	59.7															
	KZ20						9	0.8	55.0	7.4	49.5	10	11.1	42.5	5.4	81.7	10	6.1	46.3	4.1	140.2
							Mean	349.3	47.2	8.7	41.9										

Table 2. Representative chemical compositions of titanomagnetite grains. FeO* is raw data, and FeO and Fe_2O_3 were recalculated on the basis of oxide stoichiometry. The mole fractions of Ti-rich components (X_{usp}) are shown.

Sample	1 (wt%)	2 (wt%)	3 (wt%)	4 (wt%)	5 (wt%)	6 (wt%)	7 (wt%)	8 (wt%)	9 (wt%)	10 (wt%)	11 (wt%)	12 (wt%)	13 (wt%)
MgO	0.83	0.93	0.92	0.80	0.91	1.03	0.85	0.86	0.76	0.87	0.90	0.97	0.88
Al_2O_3	1.36	1.42	1.45	1.37	1.43	1.33	1.43	1.39	1.40	1.44	1.32	1.56	1.56
SiO_2	0.06	0.06	0.02	0.05	0.07	0.03	0.06	0.05	0.03	0.08	0.04	0.06	0.05
TiO_2	4.04	4.23	5.11	3.57	3.40	3.92	3.70	2.74	3.41	3.25	2.97	2.62	2.54
MnO	0.02	0.03	0.00	0.04	0.03	0.01	0.00	0.02	0.00	0.02	0.00	0.00	0.00
FeO*	87.03	87.18	87.54	88.03	88.08	88.17	88.27	88.57	88.83	89.05	89.10	89.23	89.46
Total	93.33	93.84	95.04	93.85	93.92	94.49	94.32	93.64	94.41	94.71	94.34	94.44	94.48
Recalculated													
FeO	33.58	33.76	34.94	33.36	33.13	33.54	33.62	32.51	33.50	33.34	32.88	32.56	32.63
Fe_2O_3	59.40	59.37	58.46	60.75	61.07	60.71	60.74	62.31	61.49	61.91	62.48	62.97	63.15
Total	99.28	99.79	100.90	99.94	100.03	100.57	100.40	99.88	100.57	100.91	100.60	100.75	100.81
X_{usp}	11.78	12.25	14.46	10.36	9.94	11.20	10.72	8.01	9.76	9.46	8.57	7.62	7.34

that the grains are nearly pure magnetite with a small quantity of titanium (Ti-poor titanomagnetite; Fig. 4d, Table 2). These observations can be interpreted to show that titanomagnetite is responsible for all the magnetization components observed during thermal demagnetization, apart from a minor contribution by haematite and/or maghaemite.

At each site, we refer to the first-, second-, and third-removed components during thermal demagnetization as low-, medium- and high-temperature components (green, orange and red symbols in Figs 5b–i), respectively. The difference in direction between each successive component during thermal demagnetization is largely in declination rather than inclination. The direction of the high-temperature component is westward (i.e. rotated counter-clockwise) with respect to that of the medium-temperature component. The magnitude of difference in declination ranges between 12° and 43° among eight sites (KZ2, 8, 9, 10, 15, 17, 20 and 21). In addition, the direction of the medium-temperature component is eastward (i.e. rotated clockwise) with respect to that of the low-temperature component. The amount of palaeomagnetic declination discordance ranges between 10° and 34° among these eight sites.

The unique results of thermal demagnetization that show single magnetization components from two sites of the obsidian zone (clastic layer and obsidian that contacts the clastic layer) are plotted in Fig. 5(j). The mean direction of the site in the clastic layer (KZ11) has a higher *k* value of 331.0, than the overlying obsidian sample (KZ16) that has a *k* value of 59.7. These directions show a north declination with intermediate positive inclinations similar to each other, as well as to the directions from the two sites of the crystalline zone (Figs 5a and j).

5 DISCUSSION

The thick crust of the Sanukayama lava (pumiceous and obsidian zones) reveals the presence of remanent magnetization components, each of which are isolated exclusively in thermal demagnetization. The remanent magnetization components are therefore interpreted to have been blocked at some point during the course of cooling as a thermoremanent magnetization (TRM). To clarify whether the low-, medium- and high-temperature components correspond to the temperature of deformation, it is necessary to examine the magnetic domains of remanence-carrying minerals. A magnetic domain is a domain in the magnetic material where the magnetization is in a uniform direction. If a grain contains only one magnetic domain, then it is classed as a single-domain grain. An important property of single-domain TRM is the equality of the blocking temperature during field cooling and the unblocking temperature during zero-field thermal demagnetization (Dunlop & Özdemir 1997). The remanent magnetization acquired by larger grains (i.e. multidomain grains)

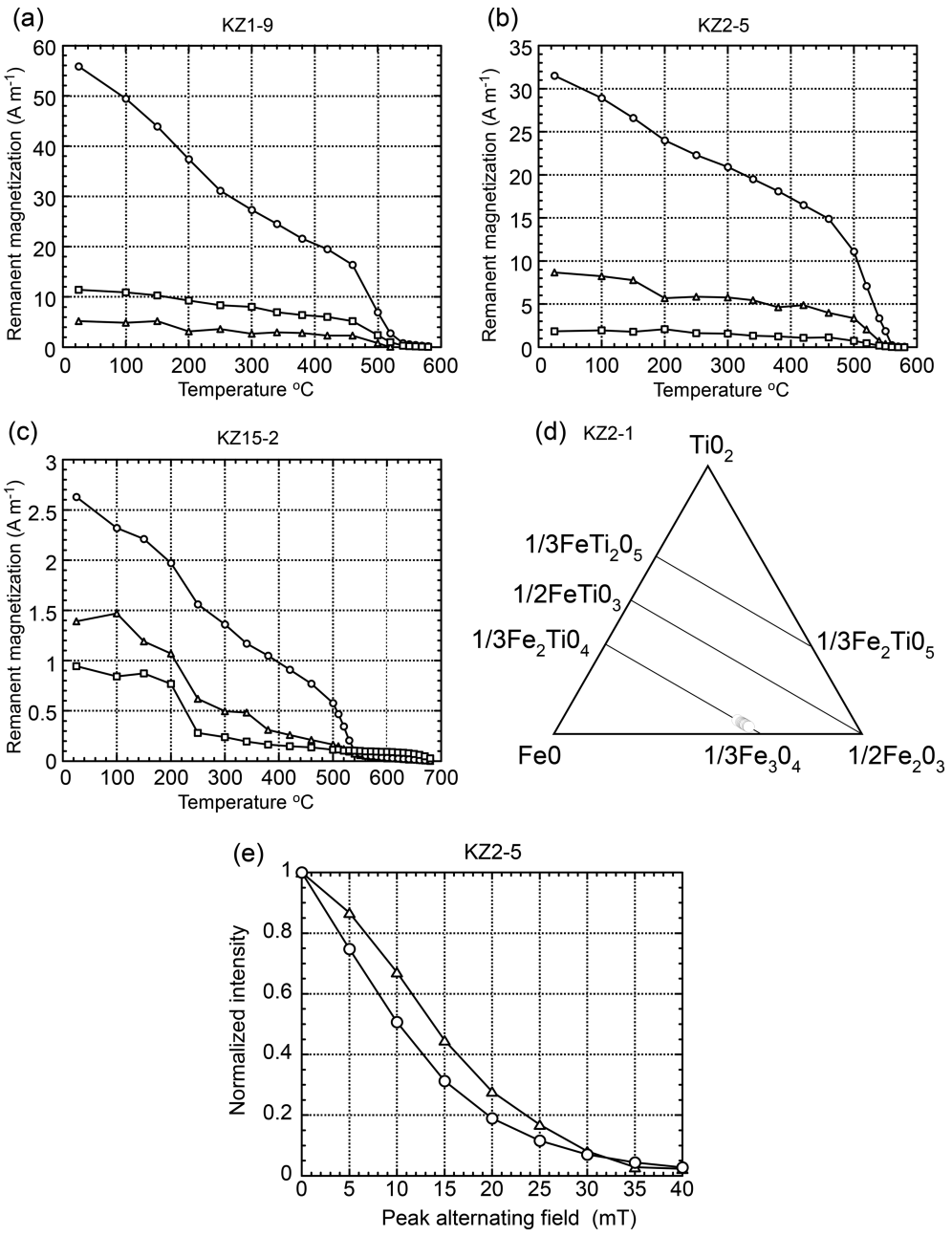

Figure 4. (a–c) Thermal demagnetization of the orthogonal three-component IRM: circles indicate the low-coercivity component of the 0.12-T field, triangles indicate the medium-coercivity component of the 0.4-T field and squares indicate the high-coercivity component of the 2.5-T field. (d) TiO_2–FeO–$1/2Fe_2O_3$ ternary diagram shows the chemical composition of iron oxides in a sample with a laboratory unblocking temperature of ~560 °C (KZ2–1). Analytical data for the iron oxides were recalculated based on oxide stoichiometry to determine Fe_2O_3 and FeO contents from the total iron content (Warner & Wasilewski 1997; Saito *et al*. 2007). Minor components are allocated as follows: $FeO = \Sigma R^{2+} = Fe^{2+} + Mg + Mn$; $Fe_2O_3 = 1/2\Sigma R^{3+} = 1/2(Fe^{3+} + Al)$; $TiO_2 = \Sigma R^{4+} = Ti + Si$. (e) The modified Lowrie–Fuller test results of obsidian sample (KZ2–5): triangles and circles indicate ARM and IRM, respectively.

does not unblock at the same temperature at which it was blocked, which produces a portion of remanent magnetization that demagnetizes above the acquisition temperature (Paterson *et al*. 2010). To demonstrate that the observed remanent magnetization is principally carried by single-domain magnetite, we have performed the modified Lowrie–Fuller test (Johnson *et al*. 1975) on an obsidian sample of site KZ2. The ARM of the sample is more resistant to AF demagnetization than the saturation IRM (Fig. 4e). ARM acquisition is enhanced for grains in the single-domain size range, in particular in the finer part of this range (Maher 1988), and therefore, the observed TRM is probably carried by single-domain magnetite. These observations are interpreted to show that the temperatures observed from remanent magnetization reflect temperatures during lava cooling or heating.

Important observations have been made: (1) the thick crust of the lava shows multiple components of remanent magnetization, whereas the inner crystalline part of the lava shows only a single component of remanent magnetization, and (2) the components

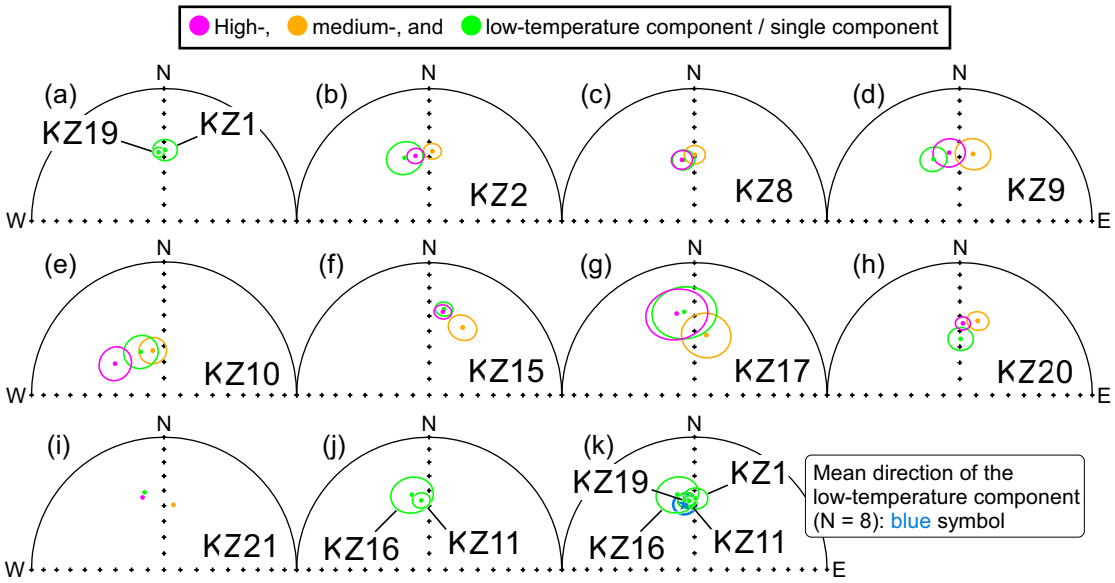

Figure 5. (a–j) Equal-area projections of site-mean directions and (k) those drawn with a mean direction of the low-temperature component from eight sites (KZ2, 8, 9, 10, 15, 17, 20 and 21).

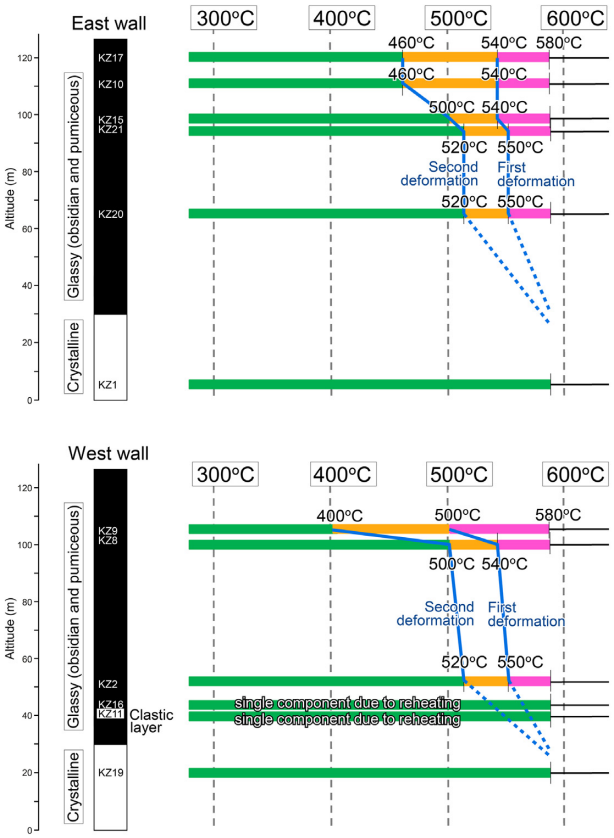

Figure 6. The temperature range over which each remanent magnetization component was isolated in each site. Each blue line denotes temperatures at the same instant.

from sampling sites located at higher elevations tend to be separated at lower temperatures during progressive thermal demagnetization. These observations are consistent on both the east and west walls, shown in Fig. 6, which also shows the separation temperature between two successive components and the number of remanent magnetization components in each site is represented by the number of colours.

Two lines have been drawn in each wall using the tie points derived from the separation temperatures of the components (blue lines, Fig. 6). This provides a basis for interpreting the occurrence of multiple components of remanent magnetization in the crust of the lava. We consider that each line represents essentially the same instant of time. That is, the thick crust records deformation at different temperatures corresponding to the elevation of the sampling sites. We suspect that the inner portion of the rhyolite lava retained its temperatures above the glass transition temperature of rhyolite and thus maintained its mobility; in contrast, the solidified crust was quickly cooled below the Curie temperature and was susceptible to deformation in response to the continued motion of lava within the inner portion of the flow. The deformation did not occur continuously throughout the cooling stages; however, we infer it to have occurred intermittently at least twice with changes in deformation orientation associated with breakout events as the lava flow field developed (e.g. Magnall *et al*. 2018). Each phase of deformation resulted in an independent magnetization component to be acquired.

Because low unblocking temperature components at crust sites are regarded to be acquired after a particular phase of deformation event, their directions would be expected to be similar to each other. The low-temperature magnetization component of the eight sites (Figs 3b–i) yields a reasonably well-defined overall mean direction of $D = 349.3$, $I = 47.2$, with $\alpha_{95} = 8.7$ (blue symbol, Fig. 3k), considered to be the ambient geomagnetic field direction at the time of lava emplacement. At the same time, the sites from the crystalline zone with single-component magnetization retained temperatures above 580 °C (blue dashed lines, Fig. 6), and thus, this part of the lava was cooled through a temperature zone where remanent magnetization was blocked. The mean direction of the low-temperature component might be close to that of the single-component magnetization if the timing of the magnetization acquisition did not differ to a large extent. We compared the direction between the two components (blue symbol versus KZ1 and 19, Fig. 3k), and they are close to each other.

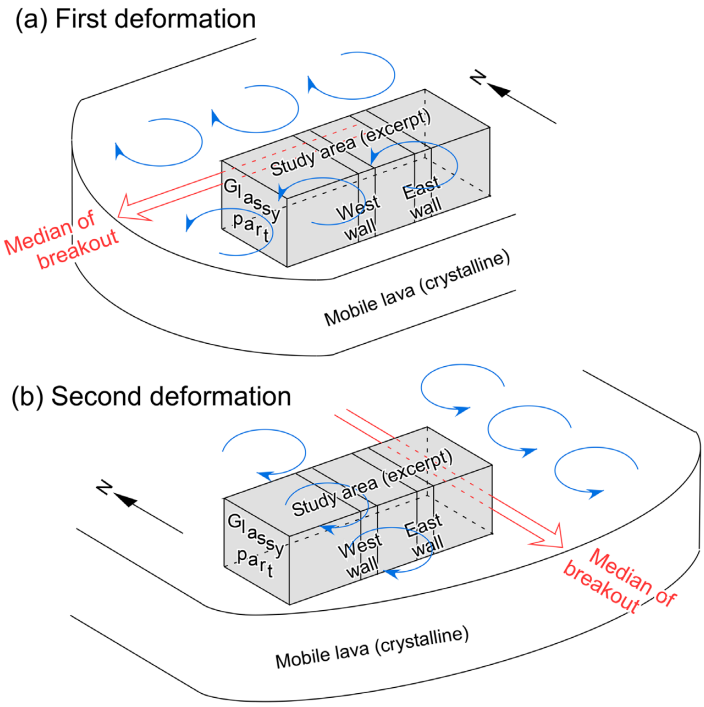

Figure 7. Schematic tectonic model for the Sanukayama rhyolite lava, illustrating the counter-clockwise rotation of the glassy part followed by clockwise rotation during its cooling.

The clastic layer that is up to 80 cm wide is located in the obsidian zone; however, this layer exhibits only a single magnetization component (Fig. 5j). The clastic layer slightly undulates, and its margin is tapered and eventually disappeared. Furukawa *et al*. (2019) analysed the clastic layer using optical microscopy and identified that this layer unexpectedly contained abundant spherulites fractured by flow-induced shear (fig. 9 of Furukawa *et al*. 2019). According to the authors, these observations suggest that the layer was formed through remobilization followed by shear-induced fracturing due to latent heat emission brought about by the formation of spherulites in this layer. The clastic layer at the location prior to spherulite formation was at temperatures >520 °C, estimated using the temperature of site KZ2 located ∼10 m above the clastic layer. This was the approximate temperature when the site experienced its second deformation. A temperature increase of at least 60 °C brings the layer to 580 °C. Spherulite growth can release considerable heat when the lava bodies are sufficiently thick, as numerically demonstrated by Tuffen *et al.* (2012). However, the temperature increase of about 60°C is not predicted from the latent heat of the small volume of the spherulite-rich zone (<80 cm wide). We suspect that in addition to latent heat by spherulite growth, frictional heating during deformation (Tuffen & Dingwell 2005) of the spherulite layer may have contributed to an increase in temperature, and associated sintering and ductile deformation of the clastic layer. The increase in melt phase H_2O due to spherulite growth may also have facilitated the reduction of the viscosity of the layer and increased the shear strain, resulting in the deformation of the spherulite layer. We argue that the clastic layer once had a remanent magnetization, probably with multiple components, but that the layer would have lost this magnetization due to latent heat and frictional heating resulting in temperatures above 580 °C that reset magnetite remanence. The reheating could affect remanent magnetization of site KZ16, an obsidian site that is in contact with the upper boundary of the clastic layer (Fig. 2b). The site yields single-component magnetization, and its direction is statistically indistinguishable from that of the clastic layer (Fig. 5j). The obsidian, at least the one adjacent to the clastic layer, has also experienced reheating that caused its initial remanent magnetization to be unblocked (Fig. 6).

The observed deformation at the crust of the lava can be ascribed to intermittent flow in its inner part that would develop into crystalline rhyolite. Direct observations suggest that this phenomenon is caused by the mechanism of rhyolite lava advancing (Tuffen *et al*. 2013; Farquharson *et al*. 2015; Magnall *et al*. 2018). The 2011 Cordón Caulle eruption in Chile enabled workers to establish how rhyolitic lava flows out extensively despite its high viscosity. The thick surface crust thermally insulates the internal flow allowing it to remain mobile long after the lava supply ceases (Anderson *et al*. 2005; Farquharson *et al*. 2015). Nevertheless, the solidified crust prevents the mobile interior from continuously advancing. Instead, the internal flow may seep out forming sporadic and intermittent breakouts at the stagnating lava margins (Tuffen *et al*. 2013; Farquharson *et al*. 2015; Fink & Anderson 2017). Magnall *et al*. (2018) reported that breakouts constituted ∼12 per cent of the total lava flow volume at Cordón Caulle; the deformation of the surface morphology due to lava flow breakout has also been observed (Tuffen *et al*. 2013). The multiple distinctive palaeomagnetic directions in our data set suggest deformation not due to continuous flowing, but due to intermittent growth of breakouts after the syn-emplacement solidification of the crust. When the lava crust studied here was cooled down to the magnetite Curie temperature, we infer that most of the lava advancement was completed but breakouts were still developing. The crustal deformation at some point in the course of cooling, detected palaeomagnetically, seemed to fit the notion of compound lava flow emplacement, involving emplacement of breakouts, as observed at the flow field generated by the 2011–2012 Cordón Caulle eruption (Tuffen *et al*. 2013; Farquharson *et al*. 2015; Magnall *et al*. 2017, 2018). Our observations are the first to adapt

the concept of flow pattern of rhyolite lava from direct observation to an ancient one.

This study results in the following implications for volcanic processes. The palaeomagnetically observed deformation was largely recognized by the deflection of the declinations (Figs 5b–i) and is accordingly interpreted as tectonic rotations about near-vertical axes. Rowland & Walker (1990), on the basis of inspection of basaltic lava flows, suggest that the lateral velocity gradient in moving lava may result in tectonic rotations of the solidified upper part of the lava about its vertical axes. We build on this model to present a tectonic model that accounts for our observations. The study area (glassy part) on the interior mobile lava was subjected to a counterclockwise torque, assuming the study area lies to the left of the median of outflow (looking downflow; Fig. 7a). Similarly, the torque administered would be clockwise if the study area were located to the right of the median (Fig. 7b). The direction of propagation of the inner portion of rhyolite lava could change, depending on the change in velocity of the flow front advance (Magnall *et al*. 2018). Our palaeomagnetic data suggest that the lava exposed at the study area advanced by taking a new path at least once in the course of cooling.

6 CONCLUDING REMARKS

Palaeomagnetism applied to an ancient rhyolite lava deposit is useful to elucidate the emplacement mechanism of the lava flow, especially because direct observations of active rhyolite lava fields are limited. Our results demonstrate that, during stages of cooling of lava, multiple components of remanent magnetization are acquired in the rhyolite lava crust, which we interpret to be a result of internal lava transport. The study is consistent with the compound flow dynamics of rhyolite inferred from direction observations of the rhyolitic lava field at Cordón Caulle, Chile, between 2011 and 2013. Internal lava may escape from its constraining crust, driving sporadic and intermittent breakouts at the stagnating, chilled lava margins.

Palaeomagnetic workers may therefore find that palaeomagnetic directions of higher-temperature components from the glassy part of rhyolite lava may not conform to the ambient geomagnetic field direction at the time of lava emplacement due to contemporaneous deformation, as implied by Ferk *et al*. (2011). It is necessary to carefully interpret the demagnetization details of remanent magnetization, particularly when using rhyolite magnetization for a range of purpose. On the contrary, low-temperature components from rhyolite lava may be acquired as a geologically stable component after complete deformation. The component is expected to retain the direction parallel to the ambient geomagnetic field direction at the time of flow emplacement.

ACKNOWLEDGEMENTS

This work was improved by comments and suggestions offered by Tadahiro Hatakeyama and Kiyoshi Fuji-ta. We are grateful to Hugh Tuffen and John W. Geissman for valued reviews of the manuscript and suggestions for improvement. Help in the field from Nao Yasuda, Mana Fukada, Yusuke Haraguchi, Daiki Uehara and Kotaro Mori is appreciated. This study was partly supported by JSPS KAKENHI Grant Numbers JP15K05313, JP15K05342 and JP19K04001.

Author contributions: KU made laboratory measurements, analysed data and wrote the manuscript. KF and TK made measurements and analysed data. KN and TK conducted field work and data analysis.

REFERENCES

Anderson, S.W. & Fink, J.H., 1990. The development and distribution of surface textures at the Mount St. Helens dome, in *Lava Flows and Domes: Emplacement Mechanisms and Hazard Implications,* pp. 25–46, ed. Fink, J.H., Springer.

Anderson, S.W., McColley, S.M., Fink, J.H. & Hudson, R.K., 2005. The development of fluid instabilities and preferred pathways in lava flow interiors—insights from analog experiments and fractal analysis, in *Kinematics and Dynamics of Lava Flows,* pp. 147–161, eds Manga, M. & Ventura, G., Geological Society of America.

Calvari, S. & Pinkerton, H., 1998. Formation of lava tubes and extensive flow field during the 1991–1993 eruption of Mount Etna, *J. geophys. Res.,* **103,** 27 291–27 301.

de Boer, C.B., Dekkers, M.J. & van Hoof, T.A.M., 2001. Rock-magnetic properties of TRM carrying baked and molten rocks straddling burnt coal seams, *Earth planet. Sci. Lett.,* **126,** 93–108.

Dunlop, J. & Özdemir, Ö., 1997. *Rock Magnetism: Fundamentals and Frontiers,* Cambridge Univ. Press, 573 pp.

Farquharson, J.I., James, M.R. & Tuffen, H., 2015. Examining rhyolite lava flow dynamics through photo-based 3D reconstructions of the 2011–2012 lava flowfield at Cordón-Caulle, Chile, *J. Volc. Geotherm. Res.,* **304,** 336–348.

Ferk, A., Leonhardt, R., von Aulock, F.W., Hess, K.-U. & Dingwell, D.B., 2011. Paleointensities of phonolitic obsidian: influence of emplacement rotations and devitrification, *J. geophys. Res.,* **116,** B12113.

Fink, J.H. & Anderson, S.W., 2017. Emplacement of Holocene silicic lava flows and domes at Newberry, South Sister, and Medicine Lake volcanoes, California and Oregon, pp. 41, U.S. Geological Survey, doi:10.3133/sir20175022I.

Fink, J.H. & Manley, C.R., 1987. Origin of pumiceous and glassy textures in rhyolite flows and domes, in *The Emplacement of Silicic Domes and Lava Flows,* pp. 77–88, ed. Fink, J.H., Geological Society of America.

Finlay, C.C *et al.*, 2010. International Geomagnetic Reference Field: the eleventh generation, *Geophys. J. Int.,* **183,** 1216–1230.

Fukuoka, H. & Iso, N., 1980. Some fission track ages of obsidians from Kozu Island, Izu, *Bull. Volcanol. Soc. Japan, Ser. 2,* **25,** 307–308.

Furukawa, K. & Kamata, H., 2005. Internal structures of Takanoobane Rhyolite lava in the western part of Aso caldera, Japan, *J. geol. Soc. Japan,* **111,** 590–598.

Furukawa, K., Uno, K., Kanamaru, T. & Nakai, K., 2019. Structural variation and the development of the thick rhyolite lava: a case study of the Sanukayama lava on Kozushima Island, Japan, *J. Volc. Geotherm. Res.,* **369,** 1–20.

Giordano, D., Russell, J.K. & Dingwell, D.B., 2008. Viscosity of magmatic liquids: a model, *Earth planet. Sci. Lett.,* **271,** 123–134.

Griffiths, R.W., 2000. The dynamics of lava flows, *Annu. Rev. Fluid Mech.,* **32,** 477–518.

Hatakeyama, T., 2018. Online plotting applications for paleomagnetic and rock magnetic data, *Earth Planets Space,* **70,** 139.

Isshiki, N., 1982. *Geology of the Kozushima District,* pp. 85, Geological Survey of Japan.

Johnson, H.P., Lowrie, W. & Kent, D.V., 1975. Stability of anhysteretic remanent magnetization in fine and coarse magnetite and maghemite particles, *Geophys. J. R. astr. Soc.,* **41,** 1–10.

Kaneoka, I. & Suzuki, M., 1970. K–Ar and fission track ages of some obsidians from Japan, *J. geol. Soc. Japan,* **76,** 309–313.

Kirschvink, J.L., 1980. The least-square line and plane and the analysis of palaeomagnetic data, *Geophys. J. R. astr. Soc.,* **62,** 699–718.

Lowrie, W., 1990. Identification of ferromagnetic minerals in a rock by coercivity and unblocking temperature properties, *Geophys. Res. Lett.,* **17,** 159–162.

Magnall, N., James, M.R., Tuffen, H. & Vye-Brown, C., 2017. Emplacing a cooling-limited rhyolite lava flow: similarities with basaltic lava flows, *Front. Earth Sci.,* **5,** 44, doi:10.3389/feart.2017.00044.

Magnall, N., James, M.R., Tuffen, H., Vye-Brown, C., Schipper, C.I., Castro, J.M. & Davies, A.G., 2018. The origin and evolution of breakouts in a cooling-limited rhyolite lava flow, *Bull. geol. Soc. Am.,* **130,** doi:10.1130/B31931.1.

Maher, B.A., 1988. Magnetic properties of some synthetic sub-micron magnetites, *Geophys. J. Int.,* **94,** 83–96.

Manley, C.R. & Fink, J.H., 1987. Internal textures of rhyolite flows as revealed by research drilling, *Geology,* **15,** 549–552.

McIntosh, W.C., 1991. Evaluation of paleomagnetism as a correlation criterion for Mogollon-Datil Ignimbrites, southwestern New Mexico, *J. geophys. Res.,* **96,** 13 459–13 483.

Paterson, G.A., Roberts, A.P., Mac Niocaill, C., Muxworthy, A.R., Gurioli, L., Viramonté, J.G., Navarro, C. & Weider, S., 2010. Paleomagnetic determination of emplacement temperatures of pyroclastic deposits: an under-utilized tool, *Bull. Volcanol,* **72,** 309–330.

Rowland, S.K. & Walker, G.P.L., 1990. Pahoehoe and aa in Hawaii: volumetric flow rate controls the lava structure, *Bull. Volcanol.,* **52,** 615–628.

Saito, T., Ishikawa, N. & Kamata, H., 2007. Magnetic petrology of the 1991–1995 dacite lava of Unzen volcano, Japan: Degree of oxidation and implications for the growth of lava domes, *J. Volc. Geotherm. Res.,* **164,** 268–283.

Suga, K., Kobayashi, K., Kanemaki, M., Miyahara, T. & Endo, K., 1992. Pyroclastic deposits in southern part of Kozushima, *Bull. Volcanol. Soc. Japan,* **37,** 71–83.

Sugihara, S. & Danhara, T., 2008. Fission track ages and description of the occurrence of obsidian sampling from Onbasejima Island and Sanukazaki Peninsula in Kozushima Island, Izu Islands, *Bulletin of Meiji University Museum,* **13,** 91–98.

Taniguchi, H., 1977. Volcanic geology of Kozu-shima, Japan, *Bull. Volcanol. Soc. Japan,* **22,** 133–147.

Taniguchi, H., 1980. Some volcano-geological significances of the hydration layer observed in the glassy groundmass of Kozu-shima rhyolite, *Bull. Volcanol. Soc. Japan,* **25,** 217–229.

Tuffen, H. & Dingwell, D., 2005. Fault textures in volcanic conduits: Evidence for seismic trigger mechanisms during silicic eruptions, *Bull. Volcanol.,* **67,** 370–387.

Tuffen, H., Cordonnier, B., Castro, J.M. & Wilson, L., 2012. Modelling the thermal effects of spherulite growth in rhyolitic lava, *AGU Fall Meeting*, Abstract V11C-2782, San Francisco, USA.

Tuffen, H., James, M.R., Castro, J.M. & Schipper, C.I., 2013. Exceptional mobility of an advancing rhyolitic obsidian flow at Cordón Caulle volcano in Chile, *Nat. Commun.,* **4,** 2709, doi:10.1038/ncomms3709.

Uehara, D., Cas, R.A.F., Folkes, C., Takarada, S., Oda, H. & Porreca, M., 2015. Using thermal remanent magnetisation (TRM) to distinguish block and ash flow and debris flow deposits, and to estimate their emplacement temperature: 1991–1995 lava dome eruption at Mt. Unzen Volcano, Japan, *J. Volc. Geotherm. Res.,* **303,** 92–111.

Warner, R.D. & Wasilewski, P.J., 1997. Magnetic petrology of arc xenoliths from Japan and Aleutian Islands, *J geophys. Res.,* **102,** 20 225–20 243.

Yokoyama, T., Shimada, A., Umemura, T. & Toyoda, S., 2004. ESR ages of rhyolitic monogenetic volcanoes in Kozushima, Japan, *Bull. Volcanol. Soc. Japan,* **49,** 23–32.

Zijderveld, J.D.A., 1967. A.C. demagnetization of rocks: Analysis of results, in *Methods in Paleomagnetism,* pp. 254–286, eds Collision, D.W., Creer, K.M. & Runcorn, S.K., Elsevier.